Available online at www.sciencedirect.com

SciVerse ScienceDirect

Ceramics International 39 (2013) 5713–5723

CERAMICS INTERNATIONAL

www.elsevier.com/locate/ceramint

Dielectric and magnetic properties of Mg–Ti substituted barium hexaferrite

Vaishali V. Soman[a,b,*], V.M. Nanoti[b], D.K. Kulkarni[c]

[a]Department of Physics, P.I.G. College of Engineering, Nagpur 440019, India
[b]Department of Physics, Priyadarshini College of Engineering, Nagpur 440019, India
[c]Department of Physics, Institute of Science, Nagpur 440001, India

Received 26 October 2012; received in revised form 26 December 2012; accepted 29 December 2012
Available online 17 January 2013

Abstract

Barium hexaferrites with general chemical formula $BaFe_{12-2x}Mg_xTi_xO_{19}$ ($x=0$, 1, 1.5, 2) were synthesized by the solid state diffusion method. X-ray diffraction (XRD) confirmed the formation of single phase magnetoplumbite with large crystallite size. The lattice parameter a decreased with the increase in x, leading to the increase in X-ray density. Formation of well defined grains was observed through scanning electron microscopy (SEM). The dielectric properties were studied by impedance measurements as a function of frequency (in the range 100 Hz–10 MHz) and temperature (in the range 30 °C–345 °C). The effect of composition, frequency and temperature on the dielectric constant (ε'), dielectric loss (tan δ), and conductivity (σ) have been explained on the basis of hopping of electrons between Fe^{2+} and Fe^{3+} ions. The variation of magnetization (M) with applied magnetic field (H) and temperature (T) were studied with a vibrating sample magnetometer (VSM). The coercivity (H_c) and saturation magnetization (M_s) decreased with the substitution level due to the occupancy of Ti^{4+} ions at octahedral site and of Mg^{2+} ions at tetrahedral site. Superparamagnetic behavior was observed in the compounds with $x=1.5$ and 2. Curie temperature decreased with the increase in x as some intersublattice exchange interactions strongly decreased with Mg and Ti addition.

Keywords: B. Electron microscopy; C. Dielectric properties; C. Magnetic properties; D. Ferrites

1. Introduction

The hexaferrites with M structure ($PbFe_{12}O_{19}$) along with its family members SrM ($SrFe_{12}O_{19}$) and BaM ($BaFe_{12}O_{19}$) have many technological applications due to the useful magnetic properties. These materials are particularly used as permanent magnets, magnetic-recording media, magneto-optical devices, microwave devices, etc. due to their high values of saturation magnetization (M_s), Curie temperature (T_c), coercivity (H_c) along with low cost, excellent chemical stability and corrosion resistance [1–3]. $BaFe_{12}O_{19}$, commonly named as M-type barium hexaferrite or simply BaM, is a ferrimagnetic material with magnetization along c-axis.

A wide range of possible compositions of these ferrites were synthesized by various preparational techniques and different substitutions [3,4]. As cation substitutions is one of the ways to modify the properties of BaM in order to meet the requirements for the specific uses, researchers have modified and improved the properties of M-ferrites by replacing Ba^{2+} by $Sr^{2+}/La^{2+}/Pb^{2+}$ ions [1,2] or substituting Fe^{3+} ions by trivalent ions like Al^{3+}, Ga^{3+}, Mn^{3+} [5,6] or with the coupled substitution of divalent cations (Zn^{2+}, Co^{2+}, Mg^{2+}, Zr^{2+}, etc.) and tetravalent cations (Ti^{4+}, Sn^{4+}, Ir^{4+}, etc.) [7–9]. In all such modified ferrites it is necessary that substituted ions maintain electrical neutrality and also have close ionic radii with the original one [9]. The extensive work carried out on the synthesis and characterization of M-type barium ferrites has been exemplified by $BaFe_{12}O_{19}$, $BaMe_xFe_{12-x}O_{19}$ (Me^{3+} = Al, Cr, Bi, Sc), $BaZn_xSn_xFe_{12-2x}O_{19}$, $BaCo_xRu_xFe_{12-2x}O_{19}$, $BaMe_xIr_xFe_{12-2x}O_{19}$ (Me^{2+} = Co, Zn), $BaMe_xTi_xFe_{11.6-2x}O_{19}$ (Me^{2+} = Co, Zn), and $BaMe_xTi_xFe_{12-2x}O_{19}$

*Corresponding author at: P.I.G. College of Engineering, Department of Physics, Digdoh, Hingana Road, Nagpur 440019, Maharashtra, India. Tel.: +91 9922299872.
E-mail address: vvsoman.aca@gmail.com (V.V. Soman).

0272-8842/$ - see front matter © 2013 Elsevier Ltd and Techna Group S.r.l. All rights reserved.
http://dx.doi.org/10.1016/j.ceramint.2012.12.089

(Me^{2+} = Co, Zn, Mn) [10]. Tehrani et al. [11] synthesized a composite of substituted hexaferrite $BaMg_{0.25}Mn_{0.25}Co_{0.5}Ti_{1.0}O_{19}$ mixed with polyvinyl chloride (PVC), as a single layer electromagnetic wave absorber in which a bandwidth of 4.5 GHz has been covered by this composition at a thickness of 2.7 mm. The authors have proposed that the material has an attractive potential in microwave applications as a radar absorbing media. Jazirehpour et al. [12] synthesized nanosized $BaFe_{12-x}Mg_{0.5x}Ti_{0.5x}O_{19}$ (x=0.0–5.0) ferrites using a 'modified sol–gel process which could provide a reliable capability for efficient substitution of elements like Ti in high substitution levels such as x=5'.

Mg–Ti substituted barium hexaferrites have applications in electronic devices. In the present study, different compositions of Mg–Ti substituted barium hexaferrites $BaFe_{12-2x}Mg_xTi_xO_{19}$ (x=0, 1, 1.5, 2), were synthesized by conventional double substitution method. Stepankova et al. [13] reported that Ti^{4+} ions preferably occupy octahedral site whereas, for Mg^{2+} ion, tetrahedral site is most favorable. Therefore the occupation of different sites by different substituent ions may exhibit different structural, magnetic as well as electrical properties. The structural and morphological studies were carried out by XRD and SEM (along with EDS). The dielectric properties were studied as a function of composition of material, temperature (T) and frequency (f). The Magnetization (M) versus magnetic field (H) measurements at room temperature and M versus T measurements at constant H were carried out with a VSM.

2. Experimental

2.1. Synthesis

The ferrites $BaFe_{12-2x}Mg_xTi_xO_{19}$ (x=0, 1, 1.5, 2) were synthesized by the solid state diffusion method. The oxides of barium (BaO), magnesium (MgO) and titanium (TiO_2) all procured from Merck and iron oxide (Fe_2O_3), procured from Sigma-Aldrich were used as the starting materials. These oxides were mixed in proper stoichiometric ratio in agate mortar with acetone (Merck) for 6 h and presintered at 900 °C for 12 h using alumina crucibles. Later, they were ground in agate mortar and finally sintered at 1300 °C for 24 h in an electronically controlled furnace. The heating rate was 6 °C/min from 30 °C to 800 °C and 4 °C/min up to 1300 °C. The cooling rate was 4 °C/min from 1300 °C to room temperature. The samples were finely crushed again and pressed into pellets of 10 mm diameter using hydraulic press (AIMIL, India). Polyvinyl acetate (PVA) (Merck) was used as binder for pellets and sintered at 1300 °C with the same heating and cooling rate.

2.2. Structural properties

X-ray diffraction study was carried out with Philips (Holland), XRD System PW1710 diffractometer with Cu target at an operating voltage 35 kV and current 20 mA with K_α line of wavelength 1.5456 Å at room temperature. The radial scans of intensity versus diffraction angle (2θ) were recorded in the range of 10° to 99° with a step size of 0.02°. Various factors which describe the crystal structure such as lattice parameters (a and c), crystallite size (D), unit cell volume (V), Miller indices (hkl), bulk density (ρ), X-ray density (ρ_x), porosity (P) were calculated. To study the morphology, the pellets were coated with gold–palladium in sputtering unit and SEM micrographs were recorded with JEOL Model JSM-6390LV (Japan) under two magnifications. The elemental identification using energy dispersive X-ray spectroscopy (EDS) was also carried out.

2.3. Dielectric properties

The dielectric measurements were carried out by Alpha-AN impedance analyzer from Novocontrol (Germany). The pellets were coated with air-drying silver paint for proper electrical contact and the study was undertaken in the temperature range 30 °C–345 °C and frequency range 100 Hz–10 MHz. The variation of dielectric constant (ε'), dielectric loss (tan δ) and ac conductivity (σ) with f, T and composition were studied.

2.4. Magnetic measurements

The Magnetization (M) versus magnetic field (H) measurements were carried out by model EV7(USA) and M versus T measurements were carried out by EG and G Princeton Applied Research (USA) with model number 150 A vibrating sample magnetometer (VSM). The saturation magnetization (M_s), remnant magnetization (M_r), coercivity (H_c) and squareness ratio (SQR) (SQR = M_r/M_s) were obtained from hysteresis curves. Curie temperature (T_c) was noted with the help of M versus T plots at constant H=1.2 T.

3. Results and discussion

3.1. X-ray diffraction studies

Fig. 1 shows XRD patterns of the ferrites $BaFe_{12-2x}Mg_xTi_xO_{19}$ (x=0, 1, 1.5, 2) having sharp and intense peaks. The formation of a single phase magnetoplumbite is confirmed as the peaks for x=0 match well with the reported values [7]. This provides an evidence that the substituted Mg^{2+} and Ti^{4+} ions replaced Fe^{3+} ions. The peaks of the host material as well as substituted ferrites appear at the same positions, but with different intensities and full width at half maximum (FWHM). These observations are attributed to the occupation of crystallographic sites of Fe^{3+} ions by substituted ions [11]. In BaM, Fe^{3+} ion occupies the sites 12k, 2a (both with spin up) and $4f_2$ (spin down) with octahedral coordination, 2b (spin up) with bipyramidal coordination and $4f_1$ (spin down) with tetrahedral coordination [14]. Mg^{2+} and Ti^{4+} ions

preferably occupy tetrahedral and octahedral sites respectively [13,15] replacing Fe^{3+} ions which may cause changes in the lattice parameters. Jazirehpour et al. [12] pointed out that the site occupancy depends upon method of synthesis and substitution level. Therefore, these peaks were indexed as a primitive hexagonal cell with space group $P6_3/mmc$ and the lattice parameters a and c for each sample have been calculated using the relation [16]:

$$d_{hkl} = \left(\frac{4}{3}\,\frac{h^2+hk+k^2}{a^2} + \frac{l^2}{c^2}\right)^{-1/2} \quad (1)$$

where (hkl) are Miller (reflection) indices of the plane whose interplanar spacing is d_{hkl}. The values of lattice parameters for the sample $x=0$ were observed to be $a=5.907$ Å and $c=23.199$ Å, which agree well with the earlier reported values [17]. On substituting Mg^{2+} and Ti^{4+} ions in $BaFe_{12}O_{19}$, the effect of the variation of Mg–Ti substitution on the lattice parameters a, c as well as on D, V, ρ, ρ_x and P have been summarized in Table 1. It can be noticed from the table that a decreases significantly for $x=1.5$ and 2 whereas c fairly remains constant for all values of x. The unit cell volume was calculated using the relation:

$$V = a^2 c \sin 60. \quad (2)$$

The volume of the unit cell for $x=0$, was found to be 701.004 $Å^3$ and decreased with the increase in x. The ionic radii of Ti^{4+}, Mg^{2+} and Fe^{3+} ions are 0.61 Å, 0.72 Å and 0.67 Å respectively [7,18,19]. Though Mg^{2+} and Ti^{4+} ions are replacing Fe^{3+} ions, the Ti^{4+} substitution seems to have a pronounced effect on the decrease in a and V. X-ray density (ρ_x) and porosity (P) were calculated using the relations:

$$\rho_x = \frac{Z\,M}{N\,V} \quad (3)$$

$$P = \left(1 - \frac{\rho}{\rho x}\right) \quad (4)$$

where, $Z=2$ is the effective number of molecules per unit cell, M = molecular weight and $N = 6.023 \times 10^{23}$/mole is the Avogadro's number.

The bulk density was observed to be lesser than the corresponding X-ray density value which is attributed to the generation of pores during sintering process [19] and the porosity was observed to increase with the increase in x. This observation can be verified from SEM micrographs given in Fig. 2. The average crystallite size was calculated using the well known Debye–Scherrer relation:

$$D = \frac{K\lambda}{\beta\cos\theta} \quad (5)$$

where, $K=0.9$, $\lambda=1.5456$ Å, β = FWHM and θ = Bragg's angle.

FWHM was calculated from prominent peaks in the XRD pattern and its average was used in this formula to get average crystallite size. D decreased with increase in concentration of Mg and Ti. For the ferrite with $x=1.5$, D was observed to be minimum, presumably as a consequence of reduction in symmetry of the crystal lattice when Fe^{3+} was being substituted by Mg^{2+} and Ti^{4+}.

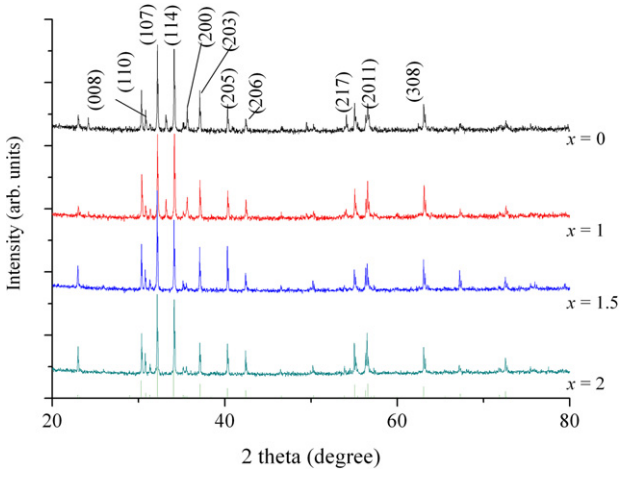

Fig. 1. X-Ray diffraction pattern of Mg and Ti substituted barium ferrite. Prominent sharp peaks are marked which show crystalline nature.

3.2. SEM with EDS characterization

SEM micrographs of substituted BaM are shown in Fig. 2. Sharp and well defined hexagonal grains in the form of plates were seen with prominent grain boundaries. The number of grains, morphology, grain boundaries changed with the composition. However, in general, the grain size varied from 0.35 μm to 0.55 μm. For the sample with $x=1$, 1.5 grains were observed to be distinctly separated but for $x=2$ grains coalesced with each other at some places to form bigger grain. Thus the grain boundaries could not be prominently seen in the sample $x=2$. The variation in the density of grain boundary could be due to the rapid crystallization process because of the introduction of Mg^{2+} and Ti^{4+} ions [20]. These observations are consistent with the results of porosity obtained from XRD

Table 1
Lattice parameters (a, c), crystallite size (D), volume of unit cell (V), bulk density (ρ), X-ray density (ρ_x) and porosity (P) of the samples with $x=1$, 1.5, 2.

Sample	a (Å)	c(Å)	D(Å)	V(Å^3)	ρ (kg/m^3)	ρ_x (kg/m^3)	P
$x=1$	5.911	23.160	685.03	700.804	3767.904	5079.128	0.258
$x=1.5$	5.068	23.162	423.90	515.234	4422.074	6781.109	0.348
$x=2$	5.012	23.158	562.60	503.898	3507.920	6803.459	0.484

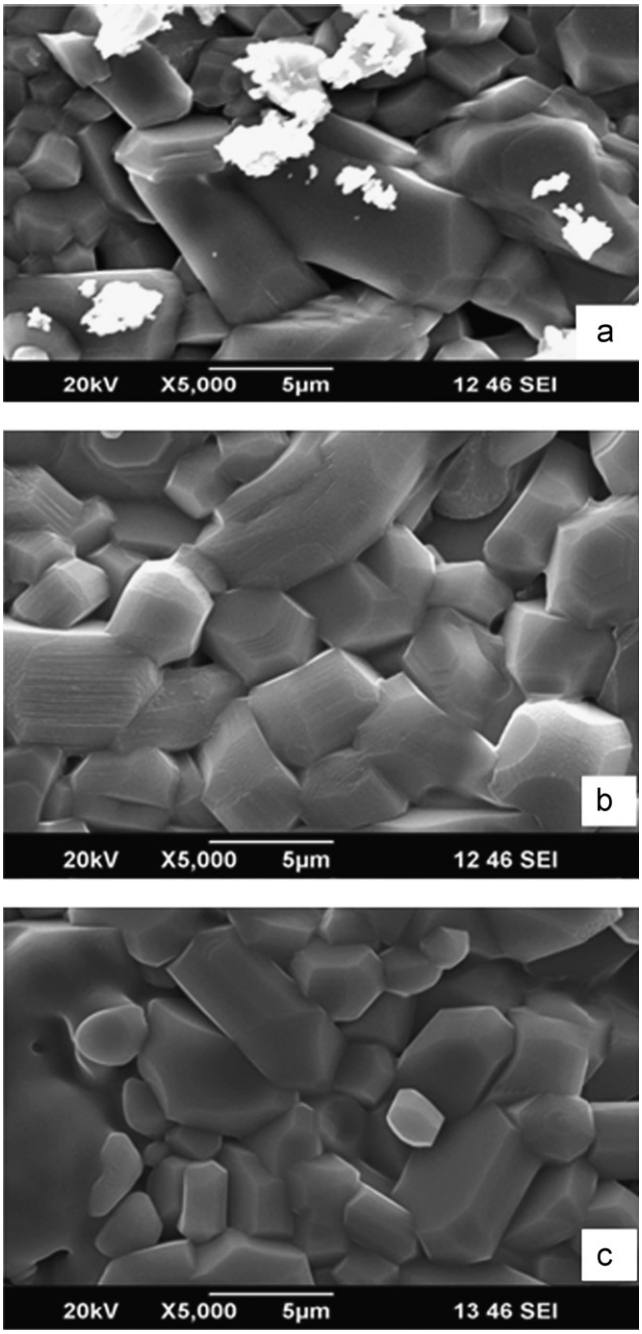

Fig. 2. SEM of ferrite with (a) $x=1$, (b) $x=1.5$, (c) $x=2$. Well formed and well separated grains can be seen.

studies. The hexagonal plates having almost the same thickness in all the three samples could be seen which indicates that the substitution level has not affected the tendency of allowing the sample to grow in a particular direction. Some pores were observed in the structure of $x=1.5$ and $x=2$ as 100% theoretical density cannot be achieved during the sintering process and hence with increase in concentration of substituent, porosity is increasing even if the volume is decreasing.

The chemical composition of the materials is identified by the EDS technique and the EDS diagram has been shown in Fig. 3. The XRD results indicate the formation of a single phase and with the identification of the constituents of the samples i.e. Ba^{2+}, Fe^{3+}, Mg^{2+}, Ti^{4+} in EDS, the replacement of Fe^{3+} ion by Mg^{2+} and Ti^{4+} can be concluded.

3.3. Dielectric properties

For understanding the mechanism of charge transfer in the ferrite matrix, the dielectric response to the change in frequency, temperature and composition were carried out with the measurement of real and imaginary parts of complex impedance (Z' and Z'' respectively) and complex dielectric constant (ε' and ε'' respectively) by impedance analyzer. The conductivity (σ) and loss tangent ($\tan\delta$) were calculated using the relations:

$$\sigma = 2\pi f \varepsilon_0 \varepsilon'' \tag{6}$$

$$\tan\delta = \frac{\varepsilon''}{\varepsilon'} \tag{7}$$

where, ε_0 is the permittivity of the free space.

For the ferrite with $x=1$, the variation of dielectric constant (ε') with frequency at some temperatures has been shown in Fig. 4 and a comparison of all compositions at room temperature is shown in Fig. 5, where a similar trend is observed for all samples. It is observed that ε' has high values ($\sim 10^3$) at lower frequency and it decreases beyond 100 kHz. This behavior is due to the existence of interfacial polarization and explained by Koops [21] on the basis of Maxwell–Wagner two layer model [22]. These ferrites have well conducting grains separated by poorly conducting thin layers of grain boundaries. The high value of ε' at lower frequencies is due to space charge polarization produced at grain boundaries. In the polarization process exchange of electrons mainly takes place between Fe^{3+} and Fe^{2+} ions for which the electrons have to pass from one grain to another through poorly conducting grain boundaries which resist their flow causing accumulation of electrons near the boundaries. This increases the space charge polarization. At higher frequencies, hopping of electrons between Fe^{3+} and Fe^{2+} ions may not take place so rapidly as that of the frequency of the applied field and therefore dispersion is observed [23]. The variation of ε' with temperature for the ferrite with $x=1$ is shown in Fig. 6. It can be seen that ε' increases with temperature almost up to 200 °C and beyond, ε' decreases gradually. For other compositions, the transition in the value of ε' is between 200 °C–250 °C which is around the T_c of ferrites particularly for $x=1.5$ and 2 (Table 2, Fig. 7). This change in ε' can be due to the magnetic transition of ferrites which are changing from ferrimagnetic to paramagnetic phase at T_c. This can also be explained on the basis of the fact that at lower temperatures the hopping of electrons between Fe^{2+} and Fe^{3+} ions induces dielectric polarization in the ferrite which in turn increases the dielectric constant. The dielectric constant seems to be systematically increasing

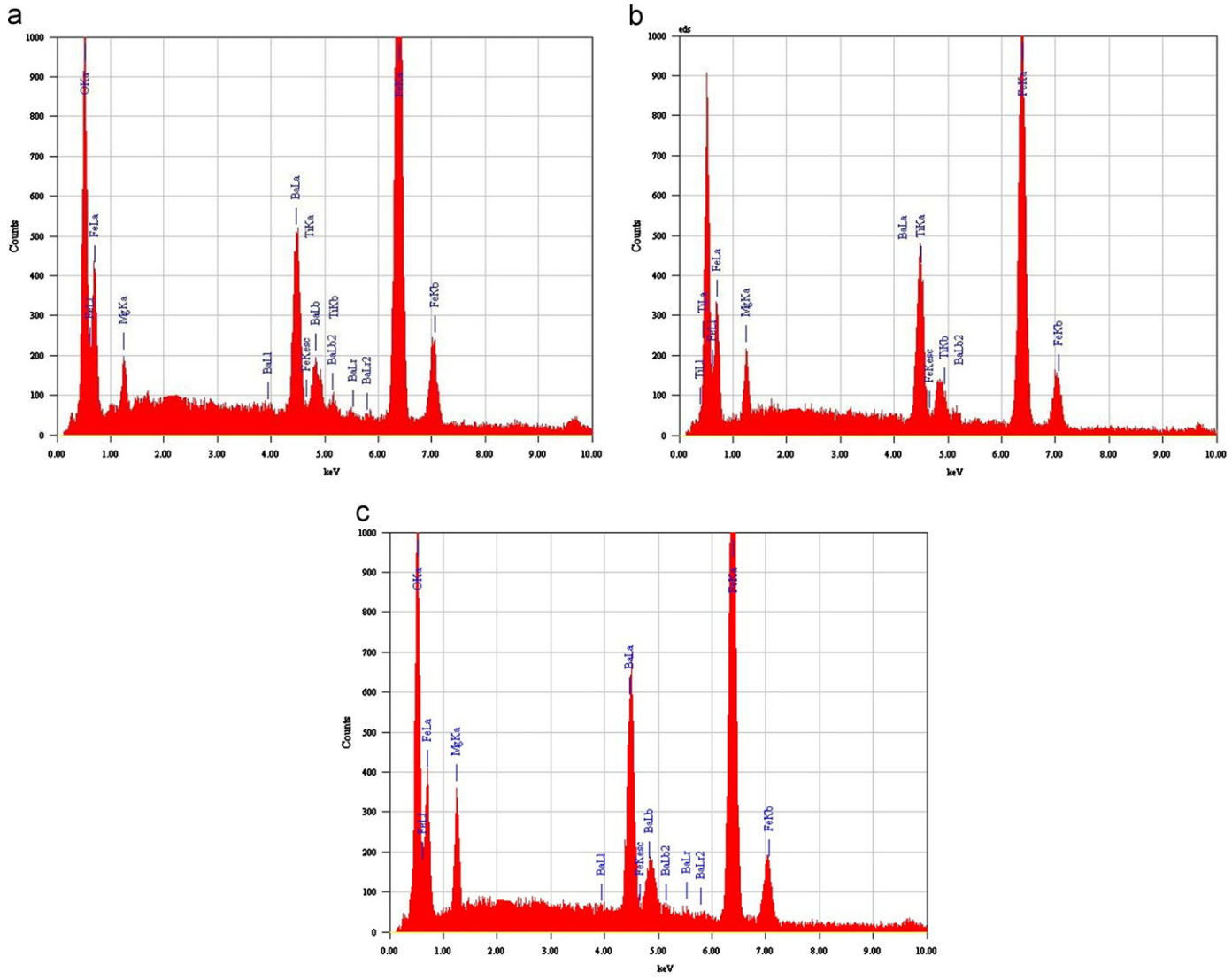

Fig. 3. EDS of ferrite with (a) $x=1$, (b) $x=1.5$, (c) $x=2$.

with the increase in temperature due to polarization and the decrease in dielectric constant at higher temperatures is due to significant increase in random vibrational motion of electrons and ions. The electric field induced magnetic field transition also depends upon the molar ratio of the phases [23].

The dielectric loss (tan δ) gives energy loss within the material during conduction of electrons. Hopping of electrons produces polarization which changes with the applied field. The dielectric loss appears when polarization lags behind the applied ac electric field which causes due to impurities and imperfections or defects in the materials. With rise in temperature the electrons and ions get thermally activated which increases the conduction and hence there is an increase in value of tan δ. As the temperature increases, the degree of dipole orientation increases and therefore energy required to overcome the barrier of the medium is reduced. This variation for $x=1$ has been shown in Fig. 8 and the comparison with other ferrites is given in Fig. 9. At a fixed temperature, energy required to overcome the barrier of the medium for conduction is fixed but the extent of orientation is decreasing with increase in frequency. Hence at higher frequency loss is smaller as compared to that at lower frequencies. The variation of tan δ with frequency at various constant temperatures, for $x=1$ is shown in Fig. 10, where a rapid decrease in dielectric loss with increase in frequency is observed. In low frequency region, more energy is required for the electron exchange between Fe^{3+} and Fe^{2+} ions due to which loss is higher. But as the frequency increases lesser energy is required for the exchange and therefore loss decreases rapidly. A comparison of change in tan δ with frequency for all the ferrite compositions at room temperature is as shown in Fig. 11. It can be seen that for $x=2$, at about 500 kHz, a peak is observed, when hopping frequency of electrons between Fe^{3+} and Fe^{2+} ions matches with frequency of external field. Due to experimental limitations, such a peak could

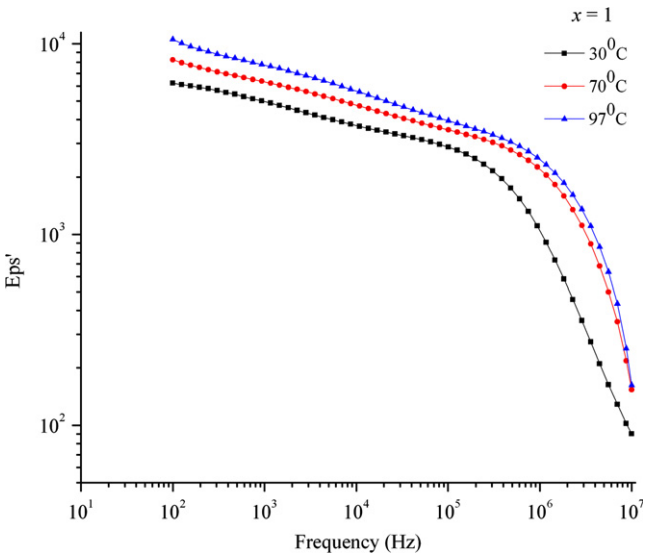

Fig. 4. Dielectric constant (ε') with frequency at some of the representative temperatures for the ferrite with $x=1$.

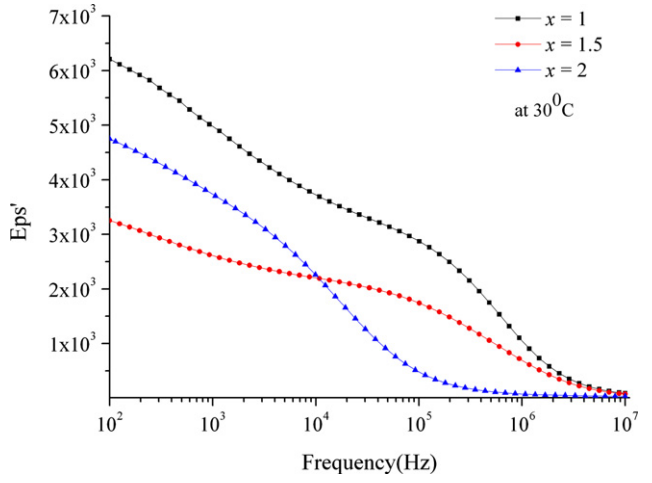

Fig. 5. Dielectric constant (ε') with frequency at 30 °C for all the compositions.

not be observed for ferrites $x=1$ and 1.5 which possibly may exist at still higher frequencies. With the increase in concentration of Mg and Ti, it was observed that the porosity increased (Table 1) and the loss tangent decreased (Fig. 11).

The variation of conductivity (σ) with frequency at constant temperatures for $x=1$ is given in Fig. 12 which shows that σ remains constant till a certain frequency f_t and beyond which an increase in conductivity is observed. It can be seen that f_t increases with the increase in temperature. The conductivity can be analyzed with Almond–West type power law [24]:

$$\sigma(\omega) = \sigma_0 + A\omega^s \tag{8}$$

where σ_0 is the frequency independent component identified as dc conductivity which depends only on temperature whereas the second term is ac conductivity which depends

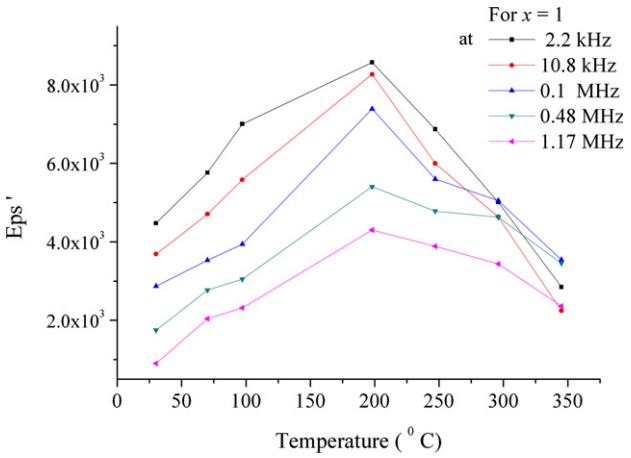

Fig. 6. Dielectric constant (ε') with temperature at some frequencies for $x=1$.

on frequency as well as temperature in a characteristic power law fashion. A and s are power law fitting parameters. The power law component s is material dependent and its value lies between 0 and 1. 'At lower frequencies, a random distribution of ionic charge carriers via activated hopping of charges gives rise to a frequency independent conductivity' [24]. With the increase in temperature the extent of random hopping decreases and s tends to1. This is observed from the dispersion in conductivity shifting towards higher frequency with increase in temperature. At lower frequency grain boundaries are effective, giving high resistance. At high frequency, grains tend to be effective good conductors and also there is increase in hopping of electrons between Fe^{3+} and Fe^{2+} ions which increases conductivity. A similar nature is observed for the ferrites $x=1.5$ and 2 which is shown in Fig. 13. It is further seen that with the increase in x the porosity increased. The increased number of pores caused hindrance to the motion of ions resulting in the decrease of conductivity. The variation of conductivity with temperature for $x=1$ and for all ferrites is as shown in Figs. 14 and 15 respectively where an increase in conductivity with rise in temperature is observed.

3.4. Magnetic properties

The M–H loops at room temperature for all ferrites $BaFe_{12-2x}Mg_xTi_xO_{19}$ ($x=0$, 1, 1.5, 2) are shown in Fig. 16. For comparison, these hysteresis curves have been redrawn in Fig. 17. The magnetic parameters calculated, such as H_c, M_s, M_r, SQR and T_c have been summarized in Table 2. For $x=0$, these values agree well with the reported results [25]. It can be seen that these magnetic parameters are decreasing with the increase in x. The ferrite BaM ($x=0$) is a hard ferrite, but with the increase in x, the H_c values decreased which indicate that the substituted ferrites are becoming soft ferrites. This is attributed to the increase in grain size as observed from SEM micrographs. The observations in the present study are

Table 2
Saturation magnetization (M_s), remnant magnetization (M_r), coercivity (H_c) and Curie temperature (T_c) of host material ($x=0$) and substituted samples ($x=1$, 1.5, 2).

Sample	M_s (emu/gm)	M_r (emu/gm)	H_c (Oe)	SQR (M_r/M_s)	T_c (°C)
$x=0$	49.08	24.35	1005	0.49	523
$x=1$	39.33	5.25	109	0.13	394
$x=1.5$	36.82	1.96	27.77	0.05	279
$x=2$	15.72	0.05	5.70	0.003	212

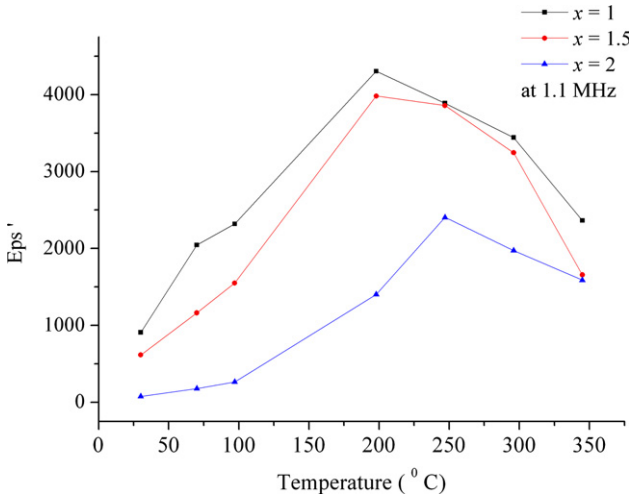

Fig. 7. Dielectric constant (ε') with temperature at 1.1 MHz for all compositions.

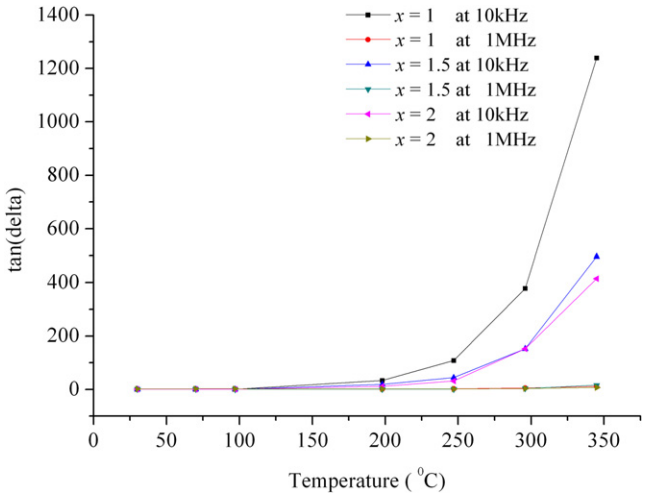

Fig. 9. Dielectric loss (tan δ) versus temperature at 10 kHz and 1 MHz for all compositions.

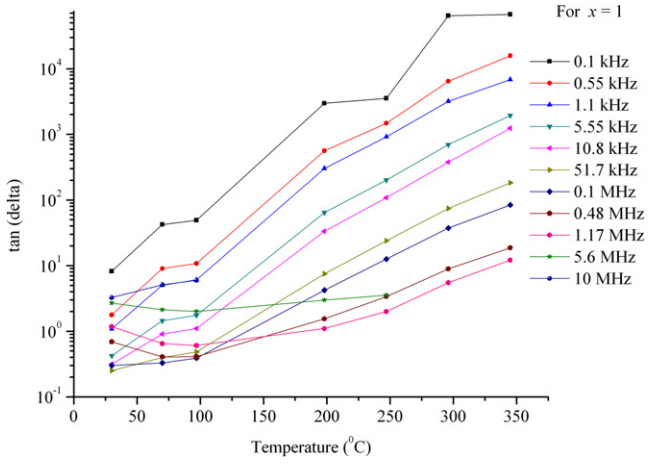

Fig. 8. Dielectric loss (tan δ) with temperature for $x=1$.

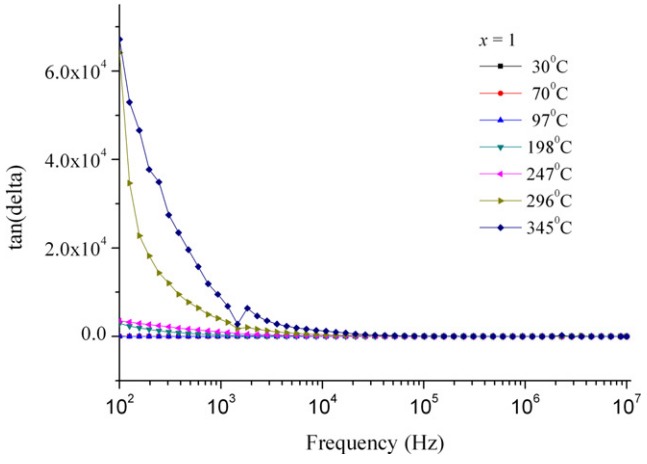

Fig. 10. Dielectric loss (tan δ) versus frequency for the ferrite $x=1$.

similar to the results obtained by Haq et al. [20] and Onreabroy et al. [2]. The observed decrease in M_s, M_r and SQR, with increase in x, can be explained on the basis of the fact that in $BaFe_{12}O_{19}$, Fe^{3+} ion occupies 12k, 2a (both with spin up) and $4f_2$ (spin down) in octahedral coordination, 2b (spin up) in bipyramidal coordination and $4f_1$ (spin down) in tetrahedral coordination. The magnetic moments with spin up orientation are parallel to overall magnetization and hence contribute to the net magnetization of the material. Ti^{4+} has strong preference for octahedral positions [15] whereas Mg^{2+} has preference for tetrahedral coordination [12]. Thus when Ti^{4+} and Mg^{2+} ions are substituted for Fe^{3+} ions, Ti^{4+} ions go to 12k or 2a octahedral sites. With the replacement of ferromagnetic Fe^{3+} ion by a nonmagnetic Ti^{4+} ion in spin up position, the net magnetization decreased. Mg^{2+} ions occupy tetrahedral $4f_1$ site of Fe^{3+} ion with spin down orientation which do not contribute to net magnetization.

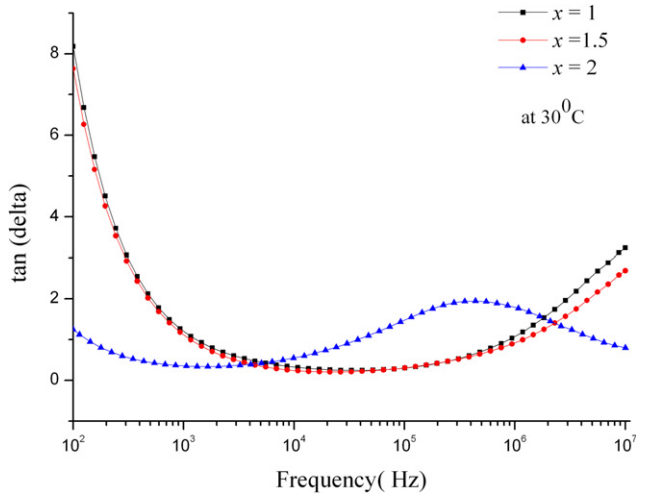

Fig. 11. Dielectric loss (tan δ) with frequency at 30 °C for all compositions.

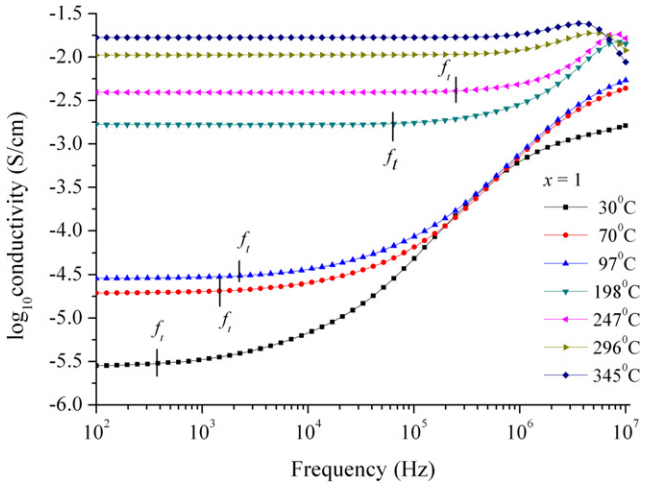

Fig. 12. log of conductivity (σ) with frequency for ferrite $x=1$.

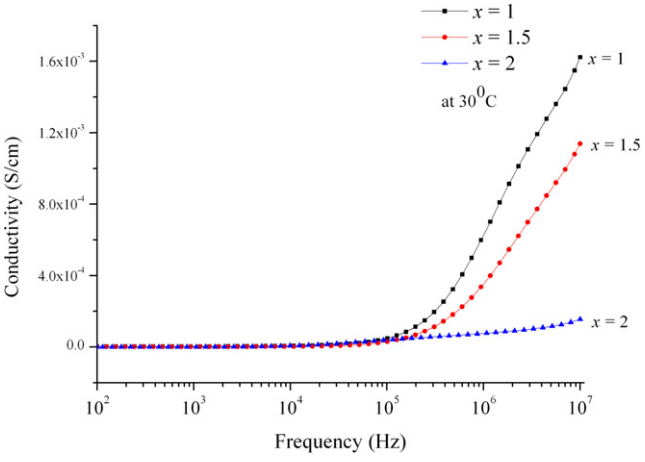

Fig. 13. Comparison of variation of conductivity (σ) with frequency at 30 °C for all the compositions.

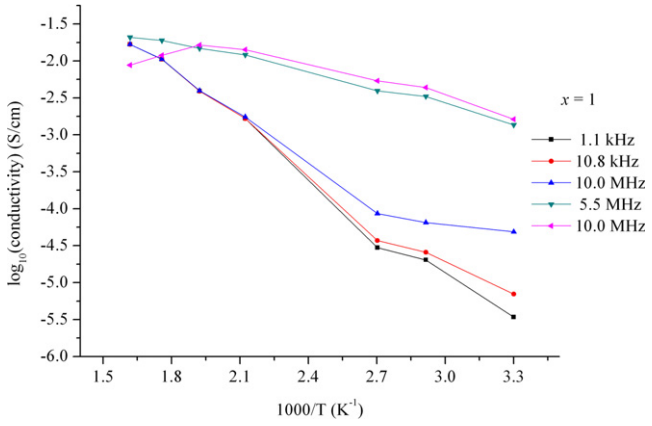

Fig. 14. Variation of log(σ) with 1000/T for the ferrite $x=1$.

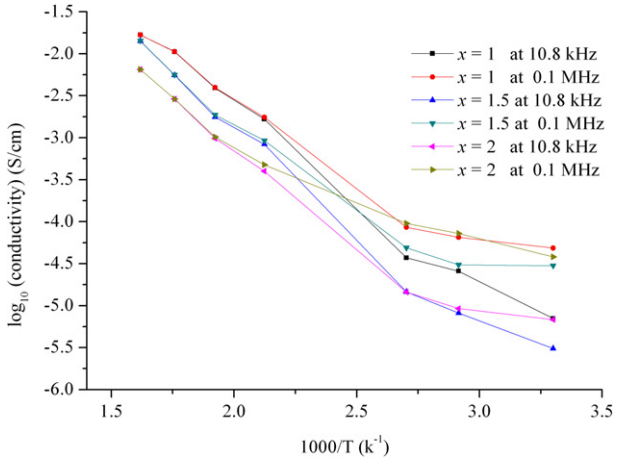

Fig. 15. Variation of log(σ) with 1000/T at 10 kHz and 0.1 MHz for all compositions.

Therefore the effect of Ti^{4+} substitution is more pronounced in reducing the values of M_s, M_r and SQR. In other words, 'with the increase in nonmagnetic substitution, the super exchange interaction causes Fe^{3+} ions in two sub-lattices of octahedral holes to have opposite spin thereby reducing M_s' [20,26]. A hard ferrite requires large coercieve field to demagnetize. Hence remnant magnetization (M_r) is large and hysteresis loop shows a large area. Thus SQR is more for hard ferrites. In the present study with increase in substitution level the ferrite is becoming soft. Hence area of hysteresis loop decreases which in turn reduces M_r and thus SQR values are very low. For the ferrite with $x=1$, the hysteresis has a very small area but for $x=1.5$ and 2, 'S' shaped hysteresis curve with non-zero magnetic moment was observed. Further for these ferrites with $x=1.5$ and 2, saturation magnetization was not attained even at highest applied field which shows superparamagnetic behavior [27].

The variation of M with T at $H=1.2$ T is shown in Fig. 18 and the values of T_c, so obtained, are given in Table 2. It is observed that T_c decreases with increase in dopant concentration. The decrease in T_c indicates that

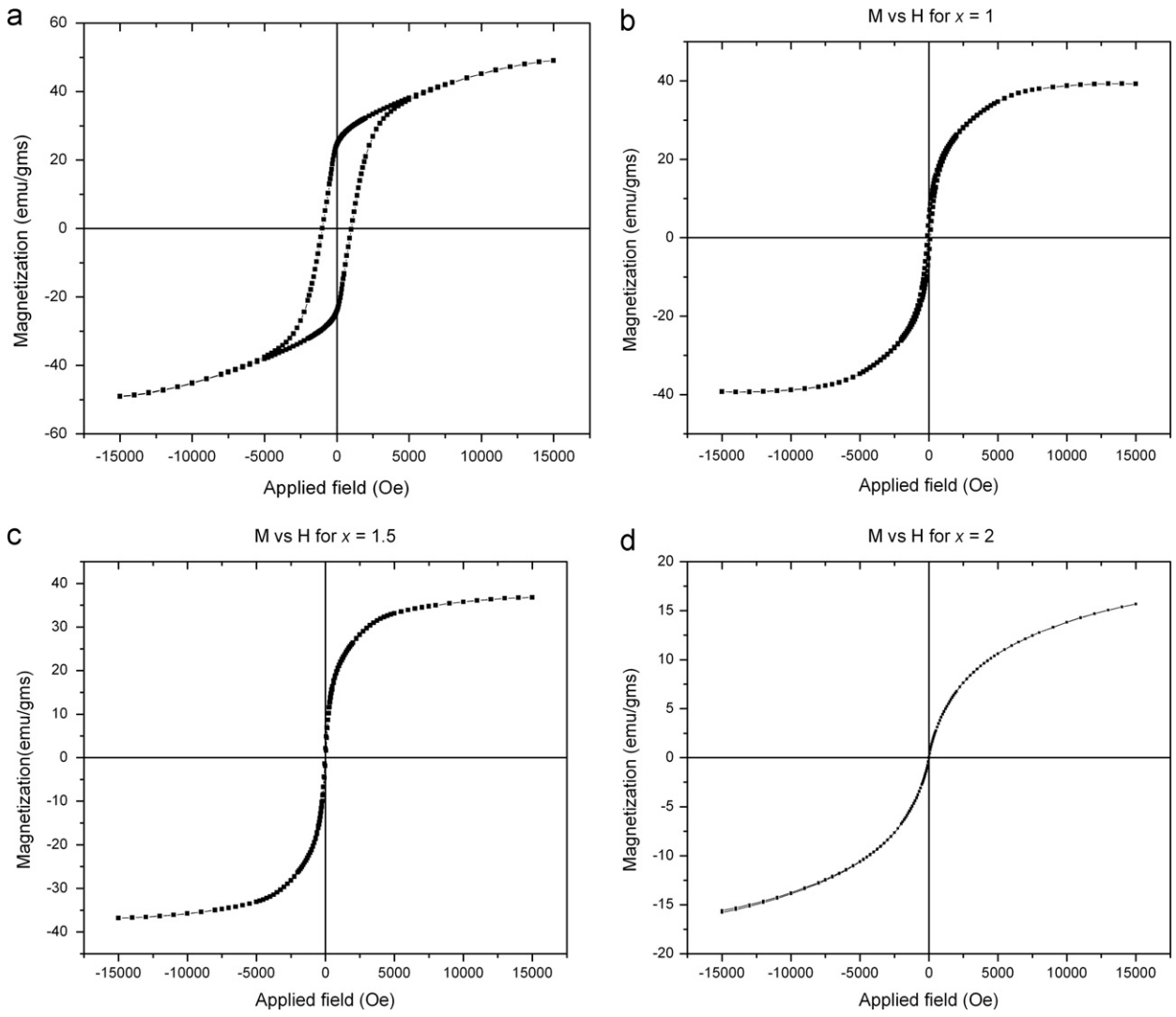

Fig. 16. M versus H plot at 30 °C for ferrites (a) $x=0$ shows hysteresis, high saturation magnetization and coercivity; (b) $x=1$ shows hysteresis of very small area with low saturation magnetization and coercivity; (c) $x=1.5$ with no hysteresis, very low saturation magnetization and coercivity and superparamagnetic nature; (d) $x=2$ with no hysteresis, not attained saturation magnetization even at highest applied field and showing superparamagnetic nature.

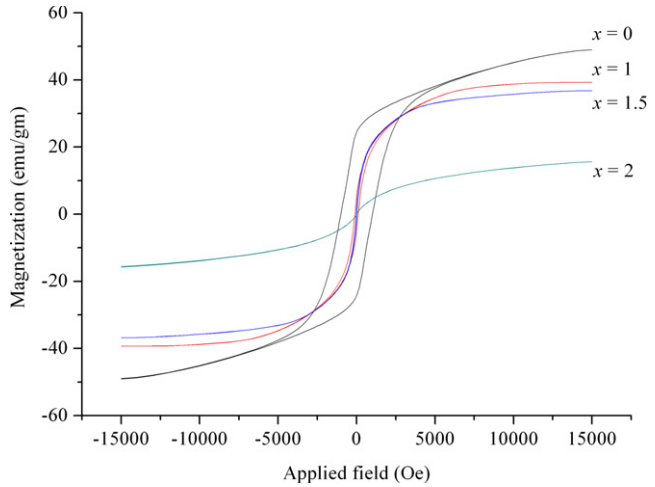

Fig. 17. Comparative M versus H of ferrites with $x=0$, 1, 1.5, 2.

some intersublattice exchange interactions are strongly diminished. The low T_c may be attributed to the presence of non magnetic ions in the tetrahedral and octahedral sites. Before reaching T_c, in case of ferrite with $x=0$, a peak is observed. With the increase in temperature, the alignment of magnetic moments change in such a way that net magnetization decreases. However, at a particular temperature below T_c, the moments freeze in a particular direction for very short duration of time due to which there is a net increase in magnetization and a peak is observed. This condition remains for a short time after which again the orientation of moments change and they align to decrease the magnetization and at T_c it becomes zero. This type of freezing is obtained in $x=0$ at 478.7 °C. It can be further seen from the M versus T curves that at room temperature the magnetization is maximum for all the samples and M decreases with further rise in T. For the

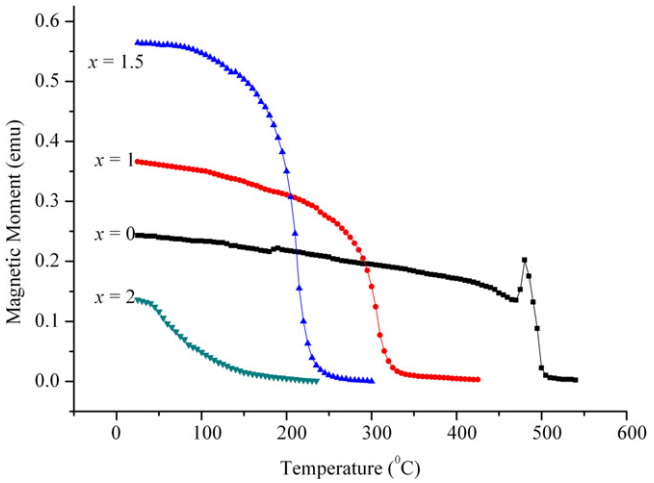

Fig. 18. M versus T of ferrites with $x=0$, 1, 1.5, 2 at constant applied field of 1.2 Tesla.

sample $x=1.5$, M was observed to be maximum as compared to all other substituted and unsubstituted samples which could be due to fact that the magnetic moments may be orienting to add up and give large values of M.

4. Conclusions

The compounds $BaFe_{12-2x}Mg_xTi_xO_{19}$ ($x=0$, 1, 1.5, 2), synthesized by conventional ceramic method were found to possess hexagonal magnetoplumbite structure of space group $P6_3/mmc$ with single phase. Replacement of Fe^{3+} ions have a significant impact on lattice parameters. XRD shows decrease in value of a as x increases and c remaining fairly constant. Crystallite size is maximum for $x=1$ and minimum for $x=1.5$. SEM micrographs support the hexagonal structure and show well formed grains and well developed grain boundaries. EDS spectra confirmed the presence of all the constituents. The dielectric properties as well as the magnetic properties are composition dependent. The variation of dielectric constant with frequency is explained on the basis of Koops model. The change in ε' with temperature is due the random vibrational motion of the electrons and ions. Dielectric loss decreases rapidly at high frequency and increases uniformly with the increase in temperature. The increase in conductivity with the rise in temperature shows the semiconductor like behavior. Magnetization versus applied field curves show hysteresis for $x=1$ and very small value of coercivity for $x=1$ while superparamagnetic nature is observed for $x=1.5$ and 2. The T_c value decreased with increase in x. For $x=0$ at a temperature below T_c, freezing of magnetic moments was obtained which increased magnetization momentarily but this could not be observed in ferrites $x=1$, 1.5, 2. Curie temperature decreased with the increase in x as some intersublattice exchange interactions strongly diminished with addition of Mg and Ti.

Acknowledgments

One of the authors VVS is thankful to IUC (Inter University Consortium), Mumbai, India, Sophisticated Test Instrumentation Centre (STIC), Kochi, India and Indian Institute of Technology (IIT), Kanpur, India, HBCSE (Homi Bhabha Centre for Science Education), Mumbai, India.

References

[1] S. Singhal, T. Namgyal, J. Singh, K. Chandra, S. Bansal, A comparative study on the magnetic properties of $MFe_{12}O_{19}$ and $MAlFe_{11}O_{19}$ (M=Sr, Ba and Pb) hexaferrites with different morphologies, Ceramics International 37 (2011) 1833–1837.

[2] W. Onreabroy, K. Papato, G. Rujijanagul, K. Pengpat, T. Tunkasiri, Study of strontium ferrites substituted by lanthanum on the structural and magnetic properties, Ceramics International 38S (2012) S415–S419.

[3] X. Zhang, Y. Duan, H. Guan, S. Liu, B. Wen, Effect of doping MnO_2 on magnetic properties for M-type barium ferrite, Journal of Magnetism and Magnetic Materials 311 (2007) 507–511.

[4] J.V.A. Santos, M.A. Macedo, F. Cunha, J.M. Sasaki, J.G.S. Duque, $BaFe_{12}O_{19}$ thin film grown by an aqueous sol–gel process, Microelectronics Journal 34 (2003) 565–567.

[5] G. Albanese, M. Carbucicchio, A. Deriu, Temperature dependence of the sublattice magnetizations in Al- and Ga-substituted M-type hexagonal ferrites, Physica Status Solidi (a) 23 (1974) 351–358.

[6] P. Sharma, R.A. Rocha, S.N. Medeiros, B. Hallouche, A. Paecsano Jr, Structural and magnetic studies on mechanosynthesized $BaFe_{12-x}Mn_xO_{19}$, Journal of Magnetism and Magnetic Materials 316 (2007) 29–33.

[7] P.A. Marino-Castellanos, A.C. Moreno-Borges, G. Orozco-Melgar, J.A. Garcia, E. Govea- Alcaide, Structural and magnetic study of the Ti^{4+}- doped barium hexaferrite ceramic samples: theoretical and experimental results, Physica B 406 (2011) 3130–3136.

[8] A. Gonzalez-Angeles, J. Lipka, A. Gruskova, J. Slama, V. Jancarik, V. Slugen, Magnetic comparison of BaCa and BaSr substituted Hexaferrite powders, Journal of Physics: Conference Series 217 (2010) 1–5.

[9] T.M. Meaz, C.B. Koch, X-ray diffraction and Mossbauer spectroscopic study of $BaCo_{0.5x}$ $Zn_{0.5x}Ti_xFe_{12-2x}O_{19}$ (M- type hexagonal ferrite) Egypt, Journal of Sol–Gel Science and Technology 26 (2003) 197–203.

[10] Z. Wenyu, Z. Qingjie, T. Xinfeng, C. Haibin, Synthesis of non-stoichiometric M-type barium ferrite nanobelt by spark plasma sintering method, Chinese Science Bulletin 50 (2005) 1404–1408.

[11] M.K. Tehrani, A. Ghesemi, M. Moradi, R.S. Alam, Wideband electromagnetic wave absorber using doped barium hexaferrite in Ku-band, Journal of Alloys and Compounds 509 (2011) 8398–8400.

[12] M. Jazirehpour, M.H. Shams, O. Khani, Modified sol–gel synthesis of nanosized magnesium titanium substituted barium hexaferrite and investigation of the effect of high substitution levels on the magnetic properties, Journal of Alloys and Compounds 545 (2012) 32–40.

[13] H. Stepankova, J. Kohout, Z. Simsa, NMR study of Ti–Co, Ti–Mg and Ti substituted hexagonal ferrites with magnetoplumbite structure, Journal of Magnetism and Magnetic Materials 104–107 (1992) 411–412.

[14] P. Wartewig, M.K. Krause, P. Esquinazi, S. Rosler, R. Sonntag, Magnetic properties of Zn- and Ti- substituted barium hexaferrite, Journal of Magnetism and Magnetic Materials 192 (1999) 83–99.

[15] M.V. Cabañas, J.M. Gonzlez-Calbet, J. Rodrı´guez¸Carvajal¸ M¨ Vallet¸Regi, The solid solution $BaFe_{12-2x}Co_xTi_xO_{19}$ ($0 \le x \le 6$): cationic distribution by neutron diffraction, Journal of Solid State Chemistry 111 (1994) 229–237.

[16] Z.H. Hua, S.Z. Li, Z.D. Han, D.H. Wang, M. Lu, W. Zhong, B.X. Gu, Y.W. Du, The effect of La–Zn substitution on the microstructure and magnetic properties of barium ferrites, Materials Science and Engineering A 448 (2007) 326–329.
[17] K.K. Mallick, P. Shepherd, R.J. Green, Dielectric properties of M- type barium hexaferrite prepared by co-precipitation, Journal of the European Ceramic Society 27 (2007) 2045–2052.
[18] Y.C. Chen, K.C. Chang, S.L. Yao, Improved microwave dielectric properties of $Nd(Mg_{0.5}Sn_{0.5})O_3$ ceramics by substituting Mg^{2+} with Zn^{2+}, Ceramics International 38 (2012) 5377–5383.
[19] M. Ahmad, F. Aen, M.U. Islam, S.B. Niazi, M.U. Rana, Structural, physical, magnetic and electrical properties of La-substituted W-type hexagonal ferrites, Ceramics International 37 (2011) 3691–3696.
[20] A. Haq, M. Anis-ur-Rehman, Effect of Pb on structural and magnetic properties of Ba-hexaferrite, Physica B 407 (2012) 822–826.
[21] C.G. Koops, On the dispersion of resistivity and dielectric constant of some semiconductors at audio frequencies, Physical Review 83 (1951) 121–124.
[22] K.W. Wagner, Annals of Physics (Leipzig) 40, 1913, 817.
[23] S.A. Lokare, D.R. Patil, R.S. Devan, S.S. Chougale, Y.D. Kolekar, B.K. Chougale, Electrical conduction, dielectric behavior and magnetoelectric effect in (x) $BaTiO_3 + (1-x)$ $Ni_{0.94}Co_{0.01}Mn_{0.05}Fe_2O_4$ ME composites, Materials Research Bulletin 43 (2008) 326–332.
[24] V.C.V. Gowda, R.V. Anavekar, Transport properties of Li_2O–MnO_2–B_2O_3 glasses, Solid State Ionics 176 (2005) 1393–1401.
[25] J. Dho, E.K. Lee, J.Y. Park, N.H. Hur, Effects of the grain boundary on the coercivity of barium ferrite $BaFe_{12}O_{19}$, Epitaxial growth of PbFe12O19 thin films by alternating target laser ablation deposition of Fe2O3 and PbO, Journal of Magnetism and Magnetic Materials 285 (2005) 164–168.
[26] A.L. Geiler, Y. He, S.D. Yoon, A. Yang, Y. Chen, V.G. Harris, C. Vittoria, Epitaxial growth of $PbFe_{12}O_{19}$ thin films by alternating target laser ablation deposition of Fe_2O_3 and PbO, Journal of Applied Physics 101 (2007) 09M510-1–09M510-3.
[27] A. Kumar, K.L. Yadav, A systematic study on magnetic, dielectric and magnetocapacitance properties of Ni doped bismuth ferrite, Journal of Physics and Chemistry of Solids 72 (2011) 1189–1194.